PINPOINTING THE POSITION OF THE POST–ASYMPTOTIC GIANT BRANCH STAR AT THE CORE OF RAFGL 2688 USING POLARIMETRIC IMAGING WITH NICMOS

David A. Weintraub,[1] Joel H. Kastner,[2] Dean C. Hines,[3] and Raghvendra Sahai[4]

ABSTRACT

We have used infrared polarimetric imaging with NICMOS to determine precisely the position of the star that illuminates (and presumably generated) the bipolar, preplanetary reflection nebula RAFGL 2688 (the Egg Nebula). The polarimetric data pinpoint the illuminating star, which is not detected directly at wavelengths ≤ 2 μm, at a position well within the dark lane that bisects the nebula, $0''55$ (~ 550 AU) southwest of the infrared peak that was previously detected at the southern tip of the northern polar lobe. The inferred position of the central star corresponds to the geometric center of the tips of the four principle lobes of near-infrared H_2 emission; identifying the central star at this position also reveals the strong point symmetric structure of the nebula, as seen both in the intensity and polarization structure of the polar lobes. The polarimetric and imaging data indicate that the infrared peak directly detected in the NICMOS images is a self-luminous source and, therefore, is most likely a distant binary companion to the illuminating star. Although present theory predicts that bipolar structure in preplanetary and planetary nebulae is a consequence of binary star evolution, the separation between the components of the RAFGL 2688 binary system, as deduced from these observations, is much too large for the presence of the infrared companion to have influenced the structure of the RAFGL 2688 nebula.

Subject headings: circumstellar matter — stars: AGB and post-AGB — stars: individual (RAFGL 2688) — stars: mass loss

1. INTRODUCTION

The bipolar structures exhibited by a substantial fraction of the known planetary nebulae likely arise during the last, rapid, preplanetary nebula (PPN) stage of evolution of intermediate-mass (1–8 $M_\odot$) stars off the asymptotic giant branch (AGB). A popular, albeit largely untested, model for such bipolarity is that the central AGB star possesses a companion that aids in the buildup of a dense, dusty equatorial torus surrounding the central star (e.g., Soker 1998). Alternatively, the fossil remnant of a β Pic–like main-sequence disk may bear responsibility for triggering bipolarity during post–main-sequence evolution (Kastner & Weintraub 1995). Whatever the mechanism that abets their formation, bipolar PPN typically show two bright reflection lobes separated by a dark dust lane. The star that illuminates the polar lobes presumably is located at or near the center of the equatorial, dust torus. While this geometry obscures the central star along our direct line of sight, photons readily escape the nebular core in the polar directions and subsequently are scattered by dust grains located primarily in the walls of the rarefied, expanding lobes. Since even the lobe walls tend to be optically thin in the near-infrared, such photons can be singly scattered out of the nebula into our line of sight. Single scattering produces polarized light that contains a record of the original direction of the unpolarized light source; therefore, polarimetric maps of such polarized nebulae contain clues as to the locations of their illuminating sources, even if those stars lie hidden inside dust lanes.

Recent direct imaging of RAFGL 2688 (the Egg Nebula) with the near-infrared camera and multiobject spectrometer (NICMOS) aboard the *Hubble Space Telescope* (*HST*) (Sahai et al. 1998) revealed a compact red source just south of the bottom of the northern reflection lobe. However, initial analysis of the polarimetric maps from NICMOS indicated that this red source was not the primary illuminator of the reflection nebulosity; this object is most likely a companion to the post-AGB star that lurks in the core of the Egg Nebula. From a preliminary examination of the 2.0 μm polarimetric map, Sahai et al. suggested that the obscured, post-AGB star was located $\simeq 750$ AU ($0''75$) south of the red companion.

In this paper, we present a rigorous analysis of the 2.0 μm polarization map of RAFGL 2688 obtained by NICMOS. We determine the precise position of the post-AGB star in the core, assess the relationship of the red source to the illuminator star, and discuss the implications of this work for understanding the formation of the Egg Nebula and of other bipolar PPN.

2. POLARIZATION DATA ANALYSIS

The data and data reduction methods used in this study were first presented by Sahai et al. (1998). In brief summary, RAFGL 2688 was imaged through the POL0L, POL120L, and POL240L filters with camera 2 (NIC2) of NICMOS, using integration times of 1215 s for each filter. These filters are centered at 1.994 μm and have a FWHM of 0.2025 μm. The field of view for these images is $19''5 \times 19''3$ and the plate scale is $0''076$ pixel^{-1} (Thompson et al. 1998). The calculations of fractional polarization, p, and polarization position angle, θ, are carried out as described by Hines

[1] Department of Physics and Astronomy, Vanderbilt University, P.O. Box 1807 Station B, Nashville, TN 37235; david.weintraub@vanderbilt.edu.

[2] Carlson Center for Imaging Science, Rochester Institute of Technology, 84 Lomb Memorial Drive, Rochester, NY 14623; jhkpci@cis.rit.edu.

[3] Steward Observatory, University of Arizona, Tucson, AZ 85721; dhines@as.arizona.edu.

[4] Jet Propulsion Laboratory, MS 183-900, California Institute of Technology, Pasadena, CA 91109; sahai@grandpa.jpl.nasa.gov.
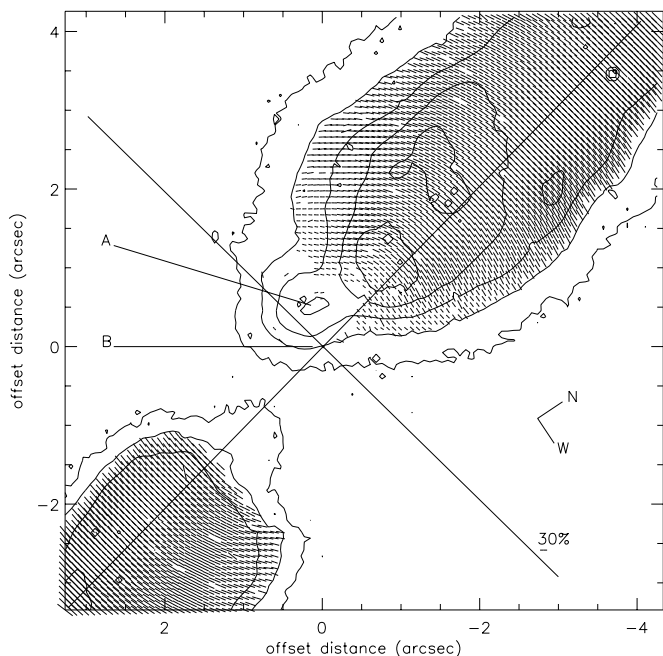
FIG. 1.—Polarization map of RAFGL 2688, obtained from 2.0 μm imaging from NICMOS. Vectors are plotted only where intensity level is greater than 3 σ in all three Stokes images. The polarimetric centroid is labeled B and found at the intersection of the lines marking the projected polar axis (12° east of north) and equatorial plane of the nebula. The intensity peak is labeled A. Vectors indicate the polarization strength (length) and position angles in each pixel, with only vectors with $p \geq 0.15$ plotted. In this and all other figures, orientation is indicated by north (N) and west (W) axes, offset distances are measured from B, absolute polarization amplitudes are indicated by a $p = 0.30$ fiducial vector marked in the lower right corner of panel, and intensity contours are drawn at 1 mag intervals, with the lowest contour at the 3 σ level in the total intensity image.

(1998)[5] (see also Hines, Schmidt, & Schneider 1999); however, we find that the best position angle calculations include the addition of a small, constant angle ϕ to θ, i.e.,

$$\theta = \frac{1}{2} \tan^{-1}\left(\frac{U}{Q}\right) + \phi \;,$$

where U and Q are the Stokes vectors obtained from the polarimetric images. The offset angle ϕ could represent a systematic rotation of the filters in the polarization filter set from their nominal position angles. For example, if the three polarizing filters were designed to lie at position angles 0°, 120°, and 240°, they actually are found at position angles $0° + \phi$, $120° + \phi$, and $240° + \phi$. Alternatively, ϕ could represent uncertainties in our knowledge of the absolute position angles assumed for the polarization calibrators. We suggest that RAFGL 2688 represents the best absolute position angle calibrator for NICMOS polarimetric data. As explained in § 4.1, we have determined empirically that $\phi = 4°.0 \pm 0°.2$. A polarization map of RAFGL 2688, made with $\phi = 4°.0$, is presented in Figure 1.

3. THE POLARIZATION STRUCTURE OF THE NEBULA

A centrosymmetric pattern is the dominant single feature of the polarization map (Fig. 1); however, it is apparent by

careful inspection of Figure 1 that the polarimetric centroid is not spatially coincident with the source (labeled A) at the southern tip of the northern lobe (see § 4). Overall, the nebula is very highly polarized, with virtually the entire southern lobe polarized with $p > 0.50$ (see Fig. 6 in Sahai et al. 1998 for a gray-scale map of the polarized intensity). A second strong feature of the polarization structure is the apparent point symmetry of the polarization pattern around position B, which we describe below. The implication of such a symmetry for the origin of the bipolar lobes is discussed later (see § 4.2).

The southern lobe is more highly polarized overall than the northern lobe (Fig. 2). In the north, only 11 pixels show vectors with polarization amplitudes above 0.7; all of these vectors are on or west of the polar axis, with all but one at least 5″ from the center of the nebula (Fig. 2a). In contrast, ~ 300 pixels in the southern lobe have $p > 0.7$; these pixels are dominantly on the eastern side of the polar axis and all of them lie more than 4″ from the center of the nebula, demonstrating a strong point symmetry to the polarization pattern around the nebular core. An additional ~ 1000 pixels are polarized with $0.6 < p < 0.7$ (Fig. 2b). In the north, virtually all of these vectors lie west of the polar axis, stretching inward along the west limb of the reflection lobe from a distance of $\sim 7″$ to just more than 3″ from the center. In the south, these vectors are uniformly spread across the lobe in the outer regions and more concentrated to the east of the polar axis closer to the core. Most of the rest of the southern lobe is polarized at a level $p > 0.50$ (Fig. 2c). In the north, the polarization vectors in the range $0.4 < p < 0.6$ cover most of the center of the lobe (Fig. 2c); the region covered by these vectors stretches radially away from the core along the eastern side; the polarization vectors in the range $0.4 < p < 0.6$ also cover the center of the southern lobe at small radial distances and then this region stretches outward from the core along the western side. Finally, the outer edges of the northern lobe nearest to the nebular core are dominated by polarization amplitudes in the 0.15–0.40 range (Fig. 2d).

4. THE POLARIMETRIC CENTROID

4.1. Method of Determination

To determine the position of the source that illuminates the nebula, we have used the method presented by Weintraub & Kastner (1993), coded into the programming software IDL. This method takes advantage of the fact that a dust grain that singly scatters photons out of the nebula imparts a polarization position angle to the scattered light that is perpendicular to the scattering plane, i.e., perpendicular to the projected direction from that dust grain to the source of illumination. Thus, for every pair of polarization vectors in a map, we can draw perpendiculars to each vector and determine a point of intersection. Ideally, for noiseless data and purely singly scattered photons, all the pairs of vectors would have a unique intersection, the *polarimetric centroid*, which should mark the intersection between the polar axis and the disk midplane (assuming the illuminating source is identical with the central star of the nebula and that the central star lies at the geometric center of the nebula).

Even for noisy data and a mixture of singly and multiply scattered photons, one can use the method of intersections of polarization perpendiculars to determine the polariza-
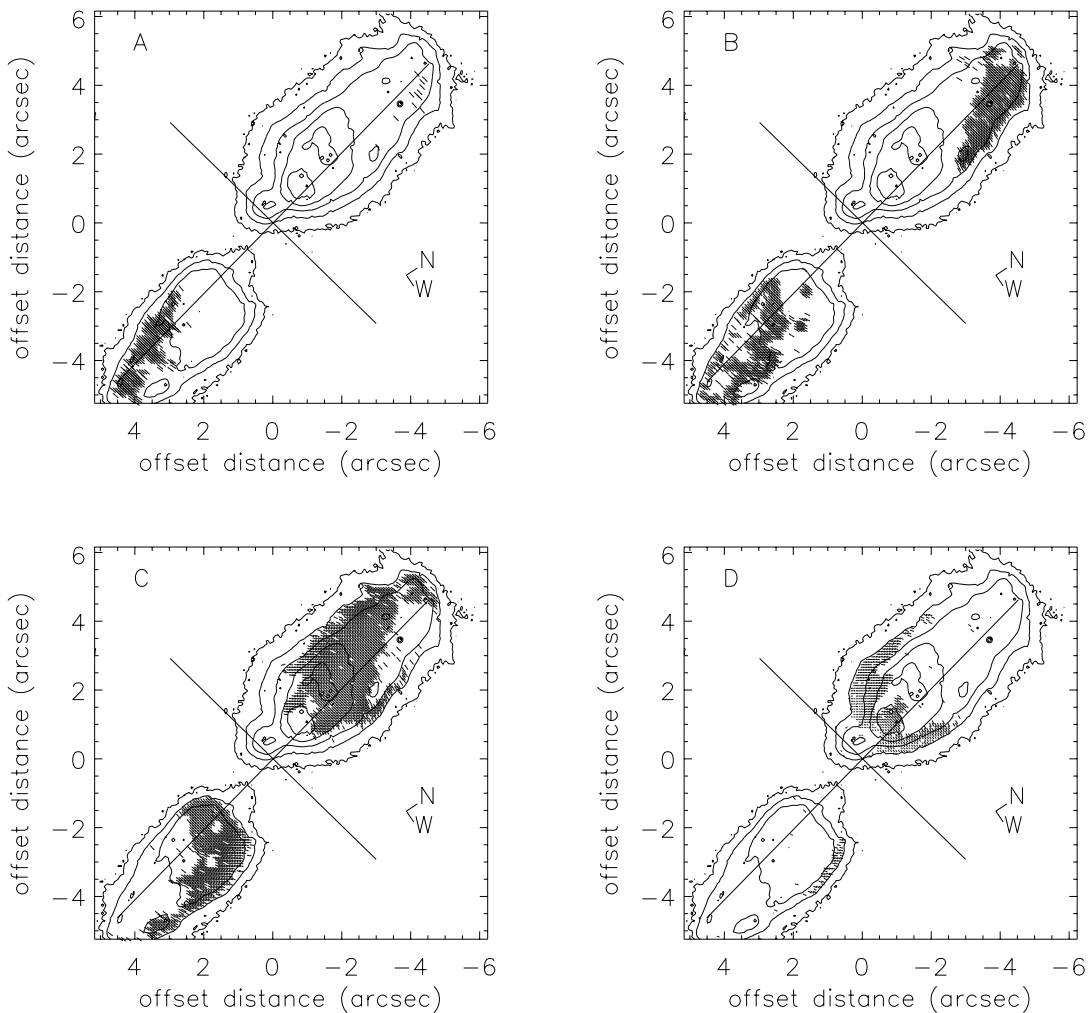
FIG. 2.—Full view of RAFGL 2688 with polarization vectors in the specified range overlaid on 2.0 μm intensity contours (same contour levels as Fig. 1). (a) $p > 0.70$, (b) $0.70 > p > 0.60$, (c) $0.60 > p > 0.40$, and (d) $0.40 > p > 0.15$.

tion centroid, albeit with finite positional error bars (Weintraub & Kastner 1993). For a given data set, the accuracy with which we can determine the centroid depends on the absolute calibration of the position angles and, thus, depends on our knowledge of ϕ. If ϕ is marginally inaccurate, the polarimetric centroid will be poorly determined, while if ϕ is quite inaccurate, there will be no polarimetric centroid in the map at all. Thus, we have determined ϕ by examining a range of ϕ values between $-10°$ and $+10°$ and adopting the value that minimizes the uncertainty in determining the polarimetric centroid. In calculating the polarimetric centroid, we limit the calculation to the more than 8000 pixels containing flux levels with signal-to-noise (S/N) ratios greater than six in all three of the POL0L, POL120L, and POL240L images.

Many of these pairs of vectors have nearly parallel position angles. For vector pairs with similar position angles, especially given even a small error in determining the true position angles, the intersection position is poorly determined. We therefore impose an additional constraint: we reject all vector pairs for which the angle between the vectors (modulo 180°) is less than 20°. This ensures that the small uncertainties in the position angle calculations do not produce large uncertainties in the actual position of the centroid. In practice, in addition to noise, many of the

pixels, usually those with polarization vectors with lower polarization amplitudes, represent parts of the reflection nebula in which multiple scattering is probably dominant. Thus, for our final calculations we placed a limit on the minimum allowable fractional polarization to be $p_{min} \geq 0.15$ in order to exclude lines of sight dominated by multiple scattering.

After calculating the intersection points for the complete set of allowable vectors and vector pairs, we calculate the statistical mean and the standard deviation of the mean, σ, for the polarization centroid. We then repeat this calculation, keeping only intersection points within a 3 σ rejection threshold of the initially determined mean. We continue with this process iteratively until the solution converges on the polarimetric centroid (denoted B). We find that the initial calculation typically lies within 0.1 pixels ($<0''.01$) of the final position and the calculation converges after only ~5 iterations and after rejecting only $\sim2\%-4\%$ of the total possible intersections. Changing the rejection threshold appears to affect only the size of the uncertainty and the rate of convergence, not the position of the polarization centroid itself.

4.2. Results

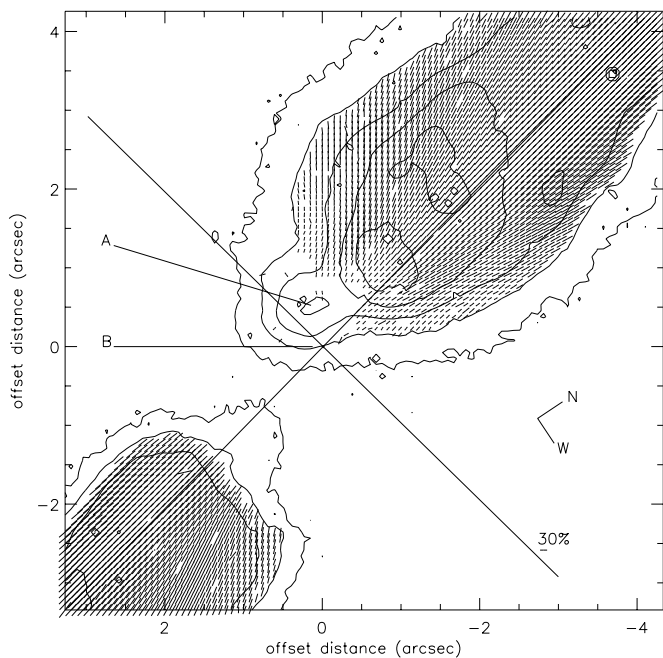In Figure 3, we present the same map as shown in Figure

FIG. 3.—Same as Fig. 1, but with all polarization vectors drawn perpendicular to their normal orientations.

1, but drawn with all of the vectors perpendicular to the polarization position angles. These vectors clearly point to a single intersection point, the polarimetric centroid (*labeled B* in Figs. 1, 3–6). In addition, this map very clearly illustrates the symmetry axis of the nebula as seen in scattered light.

By examining solutions where p_{min} ranges from 0.15 to 0.35, we find that the centroid lies $0\overset{''}{.}52 \pm 0\overset{''}{.}02$ west and $0\overset{''}{.}16 \pm 0\overset{''}{.}03$ south (Fig. 4) of the isolated intensity peak at the southern tip of the north lobe (position A), well within the dark dust lane that cuts across the middle of the bipolar
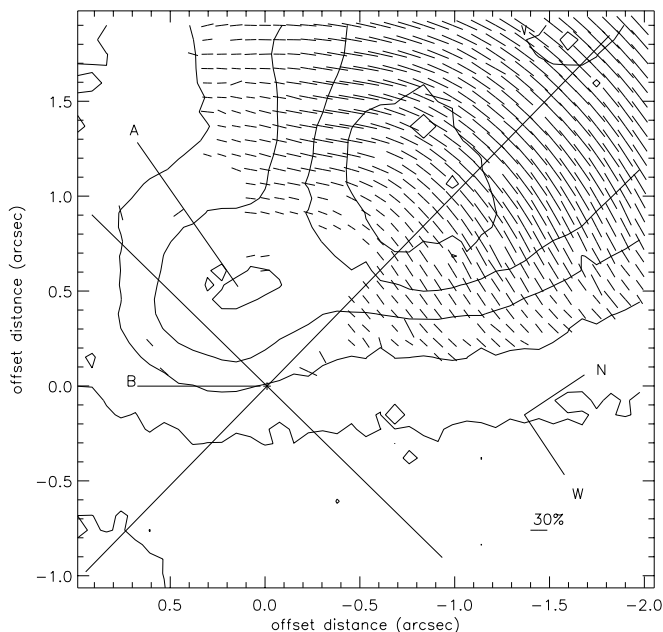

FIG. 4.—Polarization map of central region of nebula showing position of polarimetric centroid. Only vectors with $p \geq 0.15$ are plotted. Size of small plus sign at the position of source B indicates 1 σ systematic uncertainty in determination of centroid position.
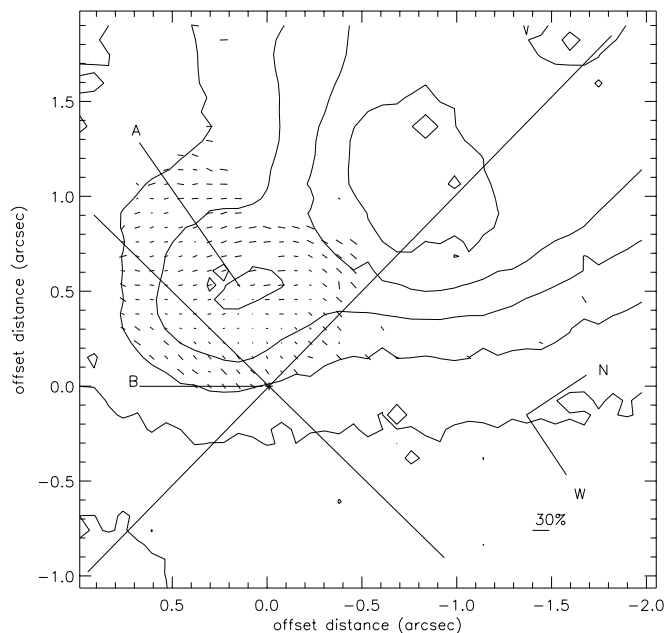

FIG. 5.—Close-up polarization map of same region as Fig. 4, but showing only vectors with $p < 0.15$.

nebula. The positional uncertainty is dominated by the systematic differences between solutions found when selecting different values of p_{min}, rather than by the statistical errors in a single calculation (which are more than an order of magnitude smaller).

We have used the position of the polarimetric centroid combined with the vector pattern to determine the direction of the projection of the polar (major) axis of the Egg Nebula. One can see (Fig. 3) that the projected polar axis, drawn at a position angle of 12° (east of north), runs exactly parallel to the straight lines formed by the alignment of the perpendiculars (of the polarization vectors) along the central axis of both the north and south scattering lobes. A change in more than 1° in the position angle of the polar axis produces a clear error in the left-right symmetry of the lobes as defined by the polarization vectors. Thus, we believe this determination of the projected position angle of the polar axis represents an improvement over the previously inferred angle of 15° (Ney et al. 1975).

In projection the centroid is located much closer to the northern than the southern lobe. The fact that B lies closer to the southern tip of the northern lobe than to the northern tip of the southern lobe is consistent with previous determinations that the polar axis of the system is inclined such that the northern lobe is tilted toward the observer. This geometry causes the optically thick equatorial torus to obscure the innermost part of the southern lobe but permits us to view most of the inner regions of the northern lobe.

It is interesting to note the point symmetry between the two scattering lobes. In the north, the majority of the total intensity of the nebula is east of the polar axis, including the brightest reflection peaks (see Fig. 1). In contrast, in the south, most of the reflection nebula is found to the west of the polar axis. In both lobes the morphologically larger side of the nebula is the side showing lower overall polarization levels. We also see that the polar axis runs through the eastern side of the inward extension of the southern lobe and through the western side of the inward extension of the

northern lobe. The simplest mechanism for producing point-symmetric structure in the nebula is the operation of collimated bipolar outflows. Sahai & Trauger (1998) have argued, based on finding a high degree of point symmetry in the morphologies of their sample of young planetary nebulae, that such outflows are the primary agent for producing aspherical structure in planetary nebulae.

5. THE ILLUMINATOR STAR AND ITS SURROUNDINGS

The polarimetric centroid presumably marks the position of the post-AGB star that illuminates most or all of both the northern and southern reflection lobes of the Egg Nebula. We now consider whether this illuminator and the intensity peak A constitute a widely spaced (>550 AU) binary system.

If a field star were at position A, such a star would reveal itself in an Airy pattern in the total intensity profile, as NICMOS generates such patterns even for very faint point sources. The absence of such a pattern indicates that the intensity peak A is an extended object. Such an object could be either a region of enhanced dust density that reflects light from B or a star embedded in the nebula that illuminates and heats the local pocket of dust around it.

In Figure 5, we present a polarization map of the same region as seen in Figure 4; however, in order to focus on the polarization behavior near A, we present in Figure 5 only the polarization vectors with amplitudes $p < 0.15$. If a point source at position A suffers little local extinction, then it becomes a source of 2 μm photons that should generate some sort of centrosymmetric polarization pattern centered on A, while the direct line of sight to A should show a low-polarization level. Given the local presence of the illuminator star at B, we might expect this pattern to be distorted by the influence of a second photon source.

In examining Figure 5, we find neither an indication of any kind of centrosymmetric pattern, even a strongly distorted one, centered on the position of the intensity peak at A, nor a simple, centrosymmetric pattern focused on the

position of the illuminator at B, similar to that which characterizes the vectors in the rest of the nebula. Instead we find, close to A, a region marked by extremely low-polarization levels and a disorganized polarization pattern, despite the fact that the S/N ratio is high. A somewhat more organized vector pattern is seen in the vectors that lie northeast, north, and northwest of A, and that appear to define a centrosymmetric pattern centered on B.

If intensity peak A were simply a region of enhanced density of cold dust, we should see a pattern of highly polarized vectors at A suggesting direct illumination from position B, as is seen at other intermediate intensity peaks further out in the northern lobe. The absence of such a pattern suggests that peak A is self-luminous; however, the lack of any Airy profile as would be expected from a point source indicates that the source at A, at 2 μm, is seen as a small, extended nebula. At this position in the nebula, the local NICMOS point-spread function generated by emission from the extended source at A, combined with the illumination of dust in this vicinity by B, generates a disorganized polarization pattern marked by relatively low polarization levels. This analysis therefore supports the suggestion that intensity peak A is a self-luminous, near-infrared source.

What is the nature of the self-luminous source at peak A? Is it a deeply embedded star or a blob of warm dust? If it is a blob of warm dust, the only likely heat sources would be illumination from the former AGB star located at least 550 AU distant or shock heating. To produce significant thermal emission at 1.65 μm, the wavelength at which the blob begins to appear (Sahai et al. 1998) would require dust with temperatures of at least 1000 K. The heating of a large amount of dust when the heat source is at least 550 AU away is highly unlikely, even for an AGB star with a luminosity of 10^4 $L_\odot$. In addition some of the luminosity of the AGB star would be expected to show up in a reflection pattern at peak A, which we do not see. As for shock heating, the maps of H_2 emission (Fig. 6; also see Sahai et al. 1998) reveal no evidence of shocked gas within a few tenths of an arcsecond (several hundred AU) of peak A. If the dust had been heated by a passing shock that is now 200 AU away, having moved past at 30 km s^{-1}, it would have had at least 30 yr to cool down. Thus, it appears more likely that intensity peak A is a star and that A and B most likely constitute a widely spaced, binary star system.

Assuming A and B are a binary, their minimum separation is 550 AU (taking $d = 1$ kpc). If A and B are both in the equatorial plane and the polar axis is tilted 15° out of the plane of the sky (Sahai et al. 1998 estimated a tilt of 10°–20° from the axial ratio of the dust torus), then the star at A would lie ~900 AU more distant than the star at B, making the true binary separation about 1000 AU. This separation is several orders of magnitude larger than that hypothesized (Morris 1987; Soker 1998) for a central binary system that could trigger the formation of an equatorial disk and the consequent bipolar outflow.

It is remarkable that position B appears to be equidistant and point-symmetrically placed between the apex of the western loop (E1), the apex of the middle of the eastern loops (E3), and the most distant points in the polar lobes of molecular hydrogen emission (Fig. 6). Thus, the polarimetric and molecular hydrogen emission centroids are positionally coincident. This result strongly indicates that the nebular illuminator at B also generated the H_2 emission,
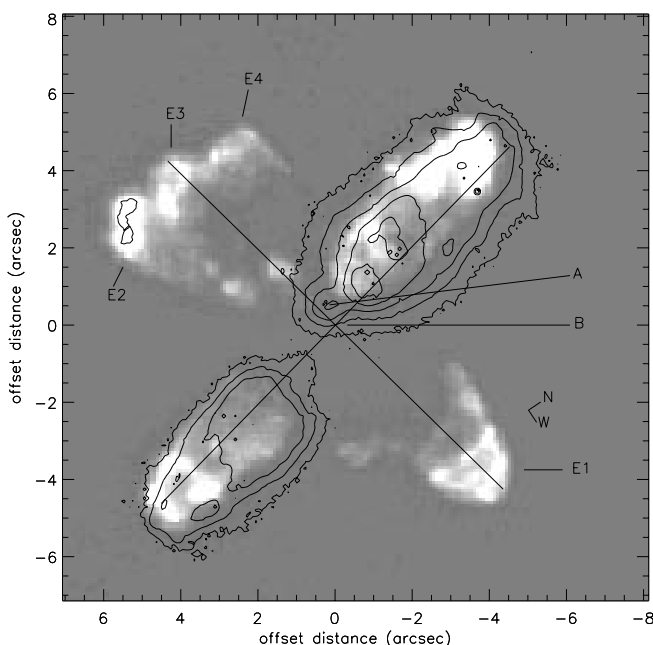

Fig. 6.—Molecular hydrogen emission (*gray scale*) overlaid with 2 μm continuum (*contours*).

where the H_2 emission regions are delineated by sharp outer boundaries suggestive of shocks. As shocks require fairly sudden changes—in this case, perhaps the rapid turning on of a fast wind from the former AGB star, perhaps triggered by the quite quick stripping and ejection of the stellar envelope and the subsequent capture of a close companion—the relationship between position B and the H_2 emission lobes suggests that the shocks seen in the H_2 were caused by a very sudden event or series of events in the evolution of the central star.

Thus, while the presence of the A + B binary at the core of RAFGL 2688 does not lend support to the binary trigger hypothesis for the formation of bipolar planetary nebulae, the relationship between the central star at B and the H_2 lobes may support such a hypothesis. Specifically, absorption of a close binary companion by the atmosphere of the central AGB star may cause the ejection of high-velocity material; the ejected material produces the shocked H_2 emission and generates the bipolar structure of the Egg Nebula.

6. SUMMARY

From a detailed analysis of the polarimetric images obtained using NICMOS and the *HST*, we have precisely determined the position of the post-AGB star in the waist of the Egg Nebula and the projected orientation of the polar axis (P.A. = 12°) of this bipolar system. This post-AGB star, which illuminates the Egg Nebula, falls point-symmetrically at the center of the molecular hydrogen emission regions that mark the waist and the polar lobes of the nebula. We find that this star lies 550 AU in projected distance, and perhaps 1000 AU in physical distance, from the star previously identified (Sahai et al. 1998) at the southern tip of the northern polar lobe. Thus, these data provide clear evidence for the presence of an optically obscured, widely spaced binary system near the core of the bipolar, pre-planetary nebula RAFGL 2688. However, the separation between these components is orders of magnitude larger than required by models postulating that companions to AGB stars trigger the production of bipolar planetary nebulae.

REFERENCES

Hines, D. C. 1998, Imaging Polarimetry with NICMOS, NICMOS Instrument Science Rep. (Baltimore: STScI)
Hines, D. C., Schmidt, G. D., & Schneider, G. 1999, PASP, in preparation
Kastner, J. H., & Weintraub, D. A. 1995. AJ, 109, 1211
Morris, M. 1987, PASP, 99, 1115
Ney, E. P., Merrill, K. M., Becklin, E. E., Neugebauer, G., & Wynn-Williams, C. G. 1975, ApJ, 198, L129

Sahai, R., Hines, D. C., Kastner, J. H., Weintraub, D. A., Trauger, J. T., Rieke, M. J., Thompson, R. I., & Schneider, G. 1998, ApJ, 492, L163
Sahai, R., & Trauger, J. T. 1998, AJ, 116, 1357
Soker, N. 1998, ApJ, 496, 833
Thompson, R. I, Rieke, M., Schneider, G., Hines, D. C., & Corbin, M. R., 1998, ApJ, 492, L95
Weintraub, D. A., & Kastner, J. H., 1993, ApJ, 411, 767